3532 *Macromolecules* **2010**, *43*, 3532–3541
DOI: 10.1021/ma9028008

Macromolecules
ARTICLE

Globule−Stretch Transitions of Collapsed Polymers in Elongational Flow Fields

Charles E. Sing and Alfredo Alexander-Katz*

Department of Materials Science, Massachusetts Institute of Technology, 77 Massachusetts Ave. Cambridge, Massachusetts 02139

Received January 1, 2010; Revised Manuscript Received February 17, 2010

ABSTRACT: Here we present our studies on the behavior of collapsed polymer chains in elongational flow fields. In particular, we present scaling and hydrodynamic simulation results on the conformation and dynamics of these macromolecules. In the noncollapsed state, we verify via our simulations that there is a smooth transition from a coil to a stretched conformation. The introduction of self-interactions or nonsolvent effects in a polymer, however, suppresses this transition up to a well-defined threshold flow rate $\dot{\epsilon}^*$ at which the chain undergoes an immediate and irreversible transition to a stretched conformation. We characterize this behavior under both freely draining and hydrodynamic interacting assumptions and develop scaling arguments to describe the globule−stretch transition in a variety of regimes. The unraveling dynamics and topologies are characterized with relation to these mechanisms, and the elongational viscosity of dilute solutions of collapsed chains is also investigated.

Introduction

There is a strong research interest in understanding the dynamic behavior of single polymer chains in solutions.[1−5] This interest has stemmed from the interest in technologies such as viscosity modification,[6] turbulence drag reduction,[1,2,7] and single-chain control in the emerging field of DNA analysis in microfluidics.[8−10] The existing literature overwhelmingly considers the behavior of polymer chains in good or Θ-solvent; however, recent results suggest that the alternative case of the dynamics of collapsed chains is also an interesting phenomenon.[11−13] For example, a combination of simulation and experimental results strongly suggest that the activity of von Willebrand factor (vWF) relies upon the hydrodynamic characteristics of collapsed globules in flows.[14,15] vWF is a globular, multimeric protein that plays a vital role in the context of clotting and coagulation in small blood vessels.[15] We expect that this sort of hydrodynamic regulation is abundant in nature, since many biological molecules are subject to self-association and hydrophobic type forces that collapse these macromolecules into subcoil dimensions.

The mechanism that facilitates this sort of behavior is very different from the classical coil−stretch transition, which in simple shear demonstrates a continuous increase of its average extension with increasing shear rate,[3,13,16] and in simple elongation demonstrates a drastic (but still continuous) increase of its average extension with increasing elongation rate.[3,6,17−21] These mechanisms rely on the entropic driving force to relax back to a coiled state, and is generally characterized by the dimensionless Weissenberg number, which compares the relaxation time of the polymer to the rate of deformation.[3,5,18,22] This opposition to stretching, however, becomes secondary to monomer−monomer interactions in the case of a collapsed polymer. The analysis of the globule−stretch transition in shear has been recently performed using simulation, which explains the presence of a sharp transition in the presence of a shear flow.[11,13] This case is particularly interesting, since the deformation of an unconstrained globule can be relaxed by rotation in the flow, and thus the absence of such a transition is predicted for droplets with a viscosity much higher than the surrounding medium.[26] Nevertheless, a transition is seen and can be predicted by considering the presence of thermal fluctuations that excite chain protrusions extending from the globular surface.[13] When the hydrodynamic drag forces overcome the restoring cohesive force, spontaneous stretching of the polymer chain occurs. This result has been considered in both the free-draining (FD) and hydrodynamic interacting (HI) cases.[13]

In this article, we present the analogous analysis for the case of a collapsed chain in an elongational flow field. Consideration of this condition allows us to more thoroughly understand collapsed polymer behavior in more complex flow geometries, as most flows can be considered to have some combination of shear and elongation. Investigation of this phenomena could further elucidate biological processes, such as blood clotting, which take place in the presence of strong flow fields. In this context, recent work has suggested that the response of collapsed biological molecules is strongly linked to gradient shear rates, which implicitly indicates a strong unfolding response of these proteins in extensional flows.[27] Also, extension represents an interesting case in and of itself, since it no longer contains the rotational components present in the shear flow that allow for the relaxation of the stresses. Instead, investigations by Stone and Leal into the elongation of droplets have shown that this energy is dissipated through the deformation of the droplet shape up to the point of spontaneous droplet breakup (or in our case, full chain elongation).[28−30] While this behavior does not seem to diverge at a maximum viscosity ratio like the shear flow case, the extension required for droplet breakup increases very quickly. Here we propose mechanisms for the transition of a polymer globule to an extended state upon application of an elongational flow, and draw analogues to the same transition upon application of a shear flow. We show that the classic coil−stretch transition is suppressed via intrapolymer interactions, and the polymer remains in a completely collapsed state until a critical extensional flow rate $\dot{\epsilon}^*$ is attained. Upon reaching this point, the coil spontaneously undergoes a globule−stretch transition. The magnitude of $\dot{\epsilon}^*$ is strongly influenced by the assumption of either the

*Corresponding author. E-mail: aalexand@mit.edu.

 Published on Web 02/26/2010

FD or HI conditions, and can be understood using simple scaling arguments. This behavior is completely analogous to the shear case, since it reasserts the result that hydrodynamic stability of polymer globules is controlled by both temperature and monomer size, which is not the case in classic droplet theories. This assertion is corroborated by nature: vWF can be considered as a polymer globule with uncommonly large "monomer" units that may facilitate the unfolding of the protein under physiological conditions.

Beyond the scaling arguments supporting our mechanism, we also analyze the dynamics and topology of the unraveling chains. This supplements the large amount of work done in recent years that has contributed to the interplay between the unfolding of coils and the so-called "molecular individualism" due to the initial chain topology.[2,4,10] This approach analyzes separately the variety of ways that coils in elongational flows can unfold, categorizing them into dumbells, half dumbells, kinks, etc. This conformational variety has profound implications on the use of bulk measurements, in particular birefringence, and other applications such as DNA sorting where the unconventional distribution induced by elongational unfolding dynamics broadens otherwise accurate measurments.[2,8] The case of collapsed polymers is less general and we show that, while some of these topologies do play a role in the extension dynamics (which tend to show the predicted exponential increase of chain length up to maximum extension), they more importantly serve to provide insight into the mechanism of the globule−stretch transition. Variation in topological effects appear to only profoundly influence the FD case when there are low interaction strengths, and both kinked and dumbell conformations appear. The protrusion and intrusion-fluctuation mechanisms presented effectively limit the dynamic pathway through which the polymer globule extends, resulting in only half-dumbell and dumbell conformations, respectively.

Finally, we investigate the elongational viscosity of a dilute solution of collapsed polymers considering a variety of conditions. This has potential impact on the field of turbulence drag reduction, which is though to be caused by the strong increase in elongational viscosity due to coil−stretch transitions in polymers.[7,23−25] There is a large amount of literature that investigates the elongational viscosity of the coil−stretch transition,[3,6,10,17,20] and we find analogous data for a collapsed polymer solution except for the appearance of a discrete jump from an otherwise elongation rate-independent viscosity to an elongation rate-independent viscosity that can be >2 orders of magnitude larger (and increases exponentially with the length of the polymer). This result provides the exciting possibility of providing drastic turbulence drag reduction or (more generally) as a way to create highly controllable discretely elongation-rate dependent viscosity fluids.

Simulation Methods

We consider the polymer to be composed of N beads of radius a interacting through a potential U. The dynamics of the ith bead position $\mathbf{r}_i$ is described by the Langevin equation:

$$\frac{\partial}{\partial t}\mathbf{r}_i = \mathbf{v}_\infty(\mathbf{r}_i) - \sum_j \mu_{ij}\nabla_{\mathbf{r}_j}U(t) + \xi_i(t) \tag{1}$$

where $\mathbf{v}_\infty(\mathbf{r})$ is the undisturbed solvent flow profile, μ_{ij} is a mobility matrix, and ξ_i is a random velocity that satisfies $\langle\xi_i(t)\xi_j(t')\rangle = 2k_BT\mu_{ij}\delta(t-t')$. For simple elongational flow the undisturbed flow profile is $\mathbf{v}_\infty(\mathbf{r}) = \dot{\varepsilon}z\hat{\mathbf{z}} - 0.5\dot{\varepsilon}x\hat{\mathbf{x}} - 0.5\dot{\varepsilon}y\hat{\mathbf{y}}$ where $\dot{\varepsilon}$ is the extensional flow rate, x, y, z are the spatial coordinates, and $\hat{\mathbf{x}}$, $\hat{\mathbf{y}}$, $\hat{\mathbf{z}}$ are the unit vectors parallel to the x, y, and z axes, respectively. We consider two different models for the description of the interaction between the polymer and the underlying fluid, which is captured through the mobility matrix μ_{ij}. The free draining (FD) case represents a "phantom chain" description where each bead of radius a feels a constant drag coefficient due to the fluid of viscosity η_S given by its stokes mobility $\mu_0 = 1/6\pi\eta_S a$. The mobility matrix thus takes the form $\mu_{ij} = \mu_0\mathbf{I}$. The hydrodynamic interaction (HI) case represents a chain in which the polymer couples with itself through the fluid. We approximate this effect by using the mobility matrix known as the Rotne−Prager−Yamakawa (RPY) tensor:[31,32]

$$\frac{\mu_{ij}}{\mu_0} = \begin{cases} \dfrac{3a}{4r_{ij}}\left(\left(1+\dfrac{2a^2}{3r_{ij}{}^2}\right)\mathbf{I} + \left(1-\dfrac{2a^2}{r_{ij}{}^2}\right)\dfrac{\mathbf{r}_{ij}\mathbf{r}_{ij}}{r_{ij}{}^2}\right) & r_{ij} \geq 2a \\ \left(1-\dfrac{9r_{ij}{}^2}{32a^2}\right)\mathbf{I} + \dfrac{3}{32}\dfrac{\mathbf{r}_{ij}\mathbf{r}_{ij}}{ar_{ij}} & r_{ij} \leq 2a \end{cases} \tag{2}$$

where $\mathbf{r}_{ij} = \mathbf{r}_i - \mathbf{r}_j$ is the vectorial distance between the ith and jth bead and $r_{ij} = |\mathbf{r}_{ij}|$. Notice that for $i = j$ one obtains the correct limit of the self-mobility of a single particle in unbounded flow, i.e., $\mu_{ij} = \mu_0\mathbf{I}$. The RPY tensor is an approximation to the full hydrodynamic interaction between two spheres and accounts to first order for the finite sphere size. Such hydrodynamic simulations have been successful in describing swollen polymers in various flows.[1,22,33] Consideration of both HI and FD conditions provides insight into the extent that hydrodynamic interactions govern the polymer dynamics in elongational flows.

The potential energy U is written as $U = U_S + U_{LJ}$. The term that accounts for the connectivity of the chain is given by[13]

$$U_S = \frac{\kappa}{2}k_BT\sum_{i=1}^{N-1}(r_{i+1,i} - 2a)^2 \tag{3}$$

where $r_{i+1,i}$ is the distance between adjacent beads along the chain, and the spring constant is taken to be $\kappa = 200/a^2$ which limits stretching of the chain to a negligible level. The second term is a Lennard-Jones potential written as:

$$U_{LJ} = \tilde{u}k_BT\sum_{ij}((2a/r_{ij})^{12} - 2(2a/r_{ij})^6) \tag{4}$$

where $\tilde{u}$ determines the depth of the potential (in units of k_BT). By varying this quantity one can tune the polymer to be swollen (small $\tilde{u}$) or collapsed (large $\tilde{u}$). To simulate the dynamics of the polymer in elongational flow, we discretize eq 1 and use a time step Δt of $10^{-4}\tau$, where τ is the characteristic monomer diffusion time $\tau = a^2/\mu_0k_BT$. All elongation rates $\dot{\varepsilon}$ are rendered dimensionless by comparison with τ, and the simulation data is always presented in terms of $\dot{\varepsilon}\tau$. It is important to note that this is not to be confused with the dimensionless Weissenberg number, $Wi = \dot{\varepsilon}\tau_R$, where τ_R is the longest relaxation time of an entire polymer coil. Averages are taken over a total number of Langevin steps of at least 2×10^7. The first 10^6 simulation steps are typically discarded for equilibration, which has been proven to far exceed the monomer conformational relaxation time within the globule.[34]

Using the full hydrodynamic matrix not only accounts for hydrodynamic interaction between monomers, but also reproduces the predicted flow stagnation inside the globule. This is demonstrated in Figure 4, where we show the average fluid velocity at position $\mathbf{r}_i$ calculated according to:

$$\langle\mathbf{v}(\mathbf{r}_i)\rangle = \mathbf{v}_\infty(\mathbf{r}_i) - \langle\sum_j \mu_{ij}\cdot\nabla_{\mathbf{r}_j}U\rangle \tag{5}$$

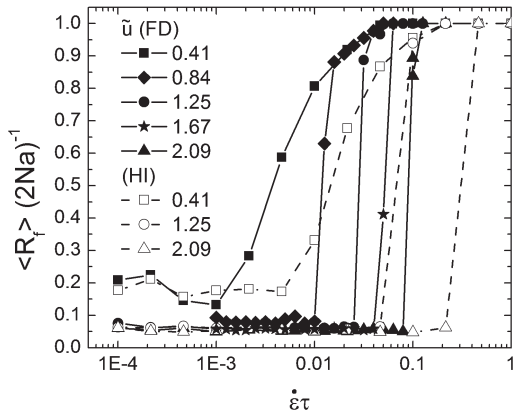

Figure 1. Average end-to-end distance ($\langle R_F \rangle$) of a polymer as a function of the elongation rate $\dot{\varepsilon}\tau$ and interaction energy $\tilde{u}$ between segments, taken from Brownian dynamics simulations of 50-bead chains. Both freely draining (solid lines, closed symbols) and hydrodynamic interaction cases (dotted lines, open symbols) are considered.

inside and outside the globule. Figure 4 also contains graphs of the deviation from the flow profile along the x and z axis due to the globule, and shows the fluid velocity approaching zero near the surface of the globule.

Results and Discussion

Elongation Flow-Induced Unfolding. Previous work in this field has demonstrated, using this same simulation method, the conditions required to obtain Θ-conditions and collapsed chains by adjusting the strength $\tilde{u}$ of the bead interaction potential.[11,13] We use the value of $\tilde{u} = 0.41$ as representative of the Θ-condition, which is where the favorable polymer−polymer interactions balance the excluded volume interactions. Increasing $\tilde{u}$ above this value results in the formation of a collapsed polymer globule, as indicated in our previous investigations into this phenomenon.[11,13]

To characterize the unfolding events in this elongational flow as a function of both chain length N, dimensionless elongation rate $\dot{\varepsilon}\tau$, and interaction energy $\tilde{u}$, we will use the magnitude of the end-to-end distance R_F as the measured variable (see the data in Figure 1). After allowing the polymer to relax to equilibrium, $\dot{\varepsilon}\tau$ is slowly increased from ca. 10^{-4} to 1. Averages of R_F are then calculated at each condition. Figure 1 shows the result for a variety of different values of $\tilde{u}$ for both the FD and HI case. The near-coiled state in FD (Figure 1, $\tilde{u} = 0.41$) demonstrates a distinct but continuous increase in size as a function of the flow rate, which agrees with the multitude of experimental and simulation results measuring this behavior.[1,2,17,17,38,40] Behavior quickly changes, however, when the interactions are strong enough to cause chain collapse. Qualitatively, as can be seen by the videos available in the Supporting Information, the observed state upon unfolding is different for elongation as it is for shear. Most importantly, while the rotational component of shear causes the chain to "tumble" and oscillate between collapsed and stretched states,[5,35] the elongation deformation is irreversible as there are no dynamical pathways to retain its collapsed state. This results in a truly discrete jump from the collapsed to stretched state, with no stable intermediate. Points on this plot that are in the intermediate zone between fully collapsed and fully stretched simply represent the average over a time period where it spent some amount of time in both states, and essentially the only time this value was attained was during the dynamic process of unfolding, which is discussed later. Also demonstrated in the movies is a small amount of shape

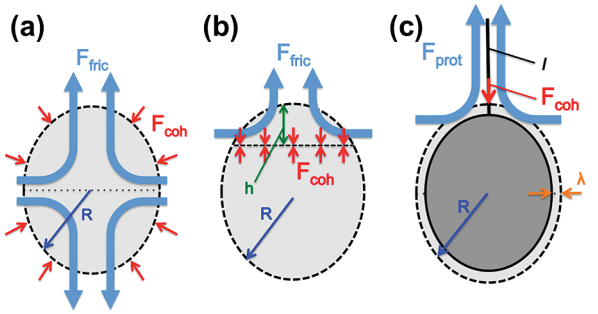

Figure 2. Schematics representing the geometries considered for the various mechanisms proposed in this article. Part a represents the FD case at low values of $\Delta\tilde{u}$. The dashed boundary to the globule, as well as the large blue flow arrows, indicate that we are considering the FD condition. Each hemisphere (separated by the dotted block line, radius R) feels an opposing drag force F_{fric}, which is counteracted by the force F_{coh} due to the surface tension (represented by the red arrows). Part b represents the FD case at high values of $\Delta\tilde{u}$. The globule now divides into two nonequivalent lobes, at a plane that is a height $h < R$ from the top of the globule. The cohesive force holding the globule together now acts along this plane, yielding a different F_{coh} (again represented by red arrows). The flow still penetrates the entire globule, but now the small lobe is the only one of interest in our analysis. Part c represents the HI case. The center of the globule now hasa solid boundary, representing the hydrodynamic screening that causes flow stagnation at the globule center. The globule now only feels the flow at the outer periphery, which is of thickness λ. The F_{coh} is now represented by a per-monomer surface tension which acts along the length of the protrusion.

deformation for the globule at high (but still sub-$\dot{\varepsilon}^*$) flow rates, however this qualitatively is small compared to the aspect ratio reported in the literature for drops before drawing occurs,[28−30] suggesting that globule−stretch transitions occur via a different mechanism. This leads us to the development of our own theory, analogous to the shear rate case, to describe the globule−stretch transition in both the FD and HI situations.

Intrusion Fluctuation Theory for FD Case. In our previous work, we introduced a protrusion nucleation scaling theory for the stretching transition for shear.[11,13] This was based upon the observation that globule unfolding in the simulations was always preceded by protrusions. This is a fundamentally different system, however, and we observe from simulations that the stretching transition can be markedly different. We first consider the FD case, which displays different behavior at high versus low interaction energies $\Delta\tilde{u}$. At low interaction energies there is a distinct lack of protrusions (or any other distinguishing topological features) and the shape of the globule is drawn into an ever-increasing ellipsoid until the chain is fully elongated (Movies S1 and S2 in the Supporting Information). Figure 2a provides a diagram of the geometry considered in the stretching mechanism for this case. We propose the characterization of this transition as the point where the elongational forces overcome the polymer surface tension. The force holding together the globule F_{coh} can, in the regime of small deformations, be written as[36]

$$F_{coh} \sim \gamma r \sim \frac{kT\Delta\tilde{u}r}{a^2} \tag{6}$$

where r is the deformed radius of the bead and $\gamma = kT\Delta\tilde{u}/a^2$ is a characteristic surface tension per bead. Here we introduce a reduced interaction energy $\Delta\tilde{u} = \tilde{u} - \tilde{u}_S$. This correction subtracts the portion of $\tilde{u}$ that accounts for the decrease in conformational entropy lost upon collapse into the globule, since γ does not contain this term. This is calculated as described by Alexander-Katz and Netz.[13]

This force competes against the drag force due to the imposed elongational velocity field, $F = v/\mu_{\text{eff}}$, where the inverse mobility μ_{eff}^{-1} must be proportional to the number of beads N (due to the free draining assumption), and the undeformed globuleradius R due to the integration of the flow field over a hemisphere: (F_{fric}):

$$F_{fric} \sim \frac{aN\eta\dot{\varepsilon}\int_V x\,\mathrm{d}V}{R^3} \sim \dot{\varepsilon}\eta NaR \tag{7}$$

At a critical elongation rate $\dot{\varepsilon}^*$, $F_{fric} = F_{coh}$:

$$\frac{kT\Delta\tilde{u}r}{a^2} \sim \dot{\varepsilon}\eta NaR \tag{8}$$

By considering small deformations where $r \sim R$, we get the following result:

$$\dot{\varepsilon}^*\tau \sim \frac{\Delta\tilde{u}}{N} \tag{9}$$

The underlying assumption of this treatment is the presence of a quick rearrangement rate such that there are negligible internal globule rearrangement times required to provide a smooth globule breakup process that is fluctuation-independent. The internal motion of the globule, however, decreases significantly upon increasing the interaction between the monomers. This yields the foundation of the other FD regime of interest, where shape deformation alone is not sufficient to cause droplet breakup. At higher interaction energies, we propose an "intrusion" nucleation theory to describe the behavior we observe in the simulations. Essentially, this theory is analogous to the behavior studied previously for shear flows,[11,13] however instead of considering fluctuations in protrusion length we consider fluctuations in the overall globule shape. The geometry for this case is schematically represented in Figure 2b. We begin by introducing a cohesive force acting upon a given plane whose normal vector is in the direction of the elongation:

$$F_{coh} \sim kT\frac{\Delta\tilde{u}(hR)^{1/2}}{a^2} \tag{10}$$

where $h < R$ is the distance along the elongation direction from the top of the globule to the plane. The portion $kT\Delta\tilde{u}/a^2$ is analogous to the γ term in eq 6, while the $(hR)^{1/2} \approx (R^2 - (R-h)^2)^{1/2}$ portion represents the circumference of the plane over which γ is acting. This plane divides the globule into two nonequivalent lobes. This force is counteracted by the drag force that is pulling the two lobes (for simplicity, we analyze the smaller lobe as indicated in Figure 2b):

$$F_{prot} \sim \frac{\dot{\varepsilon}N_s}{\mu_0}\frac{\int_{R-h}^{R} z(R^2-z^2)\,\mathrm{d}z}{\int_{R-h}^{R}(R^2-z^2)\,\mathrm{d}z} \sim \frac{\dot{\varepsilon}\eta R^2h^2}{a^2} \tag{11}$$

where x is the elongation direction, and $N_s \sim \int_{R-h}^{R}(R^2 - z^2)\,\mathrm{d}z/a^3$ number of beads in the portion of the globule above the plane at height h. From the equipartition of thermal energy, it follows that $h^2 \sim R^2\Delta\tilde{u}^{-1}$ (a comparison of the cohesive energy of the excess surface area $4\pi h^2$ due to lobe creation versus the original surface area of the globule $4\pi R^2$). We can then set $F_{prot} = F_{coh}$ and obtain the following result:

$$\dot{\varepsilon}^*\tau \sim \frac{\Delta\tilde{u}^{7/4}a^3}{R^3} \sim \frac{\Delta\tilde{u}^{7/4}}{N} \tag{12}$$

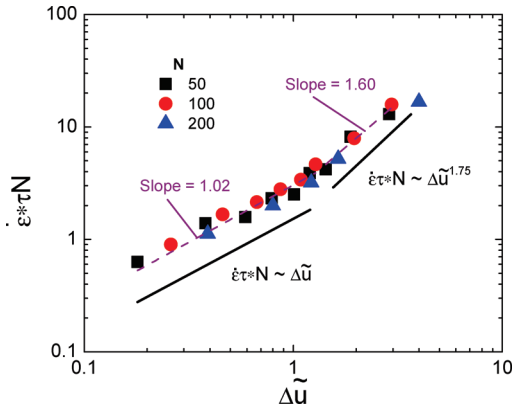

Figure 3. The scaling behavior of the critical elongation rate $\dot{\varepsilon}^*\tau$ versus the interaction energy $\Delta\tilde{u}$ taken from Brownian dynamics simulations for chains of varying length using the FD assumption. Two scaling regimes areseen, with $\dot{\varepsilon}^* \sim \Delta\tilde{u}^1$ at low interaction energies and $\dot{\varepsilon}^* \sim \Delta\tilde{u}^{1.75}$ at high interaction energies. Results are shown for $N = 50$ (black squares), $N = 100$ (red circles), and $N = 200$ (blue triangles). The dashed purple lines represent the best fit lines through the data, while the solid black lines demonstrate the slope predicted by the scaling argument. The slopes for the best fit lines are in excellent agreement with the theoretical prediction.

This model considers that there are random thermal breakups and formations of the globule, similar to capillary instabilities. If these separate the globule into large enough "nodes", the cohesive nature of the globule will be compromised and it will extend. Essentially this is similar in spirit to the protrusion mechanisms, only in the extreme that the protrusions are large and are formed "underneath" the usual globule surface. An example of this behavior can be seen in Movie S3 (Supporting Information). It is instructive to notice the transition point between these two models, which occurs at ca. $1kT$. This is the point at which $h^2/R^2 \sim 1$, so the breakup is no longer limited by the fluctuations in intrusion lengh (typical intrusions will span the entire globule radius)at lower interaction strengths and the $\dot{\varepsilon}^*\tau \sim \Delta\tilde{u}^1$ scaling is obtained.

As shown in Figure 3, both of these theories are supported by the simulation results. The highest elongation rate at which the globule appears collapsed in Figure 1 is plotted as the dimensionless critical elongation rate $\dot{\varepsilon}^*\tau N$ ona log−log plot (Figure 3) versus the interaction energy, $\tilde{u}$. The scaling of the flow rate with the interaction energy consistently follows the predicted $\dot{\varepsilon}^* \sim \tilde{u}^1$ relationship for low interaction energies, and the predicted $\dot{\varepsilon}^* \sim \Delta\tilde{u}^{7/4}$ relationship for high interaction energies. The N scaling is used to reduce the critical elongation rate, and the subsequent collapse of the curves onto one single universal curve corroborates our scaling arguments in this respect as well. The N scaling provides the intuitive result that large polymer globules require less flow rate to undergo a globule−stretch transition. Finally, given the definition of $\tau = a^2/(\mu_0 k_B T) = 6\pi\eta a^3/(k_B T)$, we obtain the result that $\dot{\varepsilon}^* \sim a^{-3}$ for both high and low interaction energy regimes. This corroborates the result obtained in previous work that suggests that the size of the monomer is an important factor in determining the stretch transition, and is a possible reason for the structure of proteins such as vWF (which has a monomer size on the order of 100 nm).[11,13,14]

Protrusion Nucleation Theory for HI Case. Upon consideration of hydrodynamic interactions in the unfolding behavior of collapsed polymer globules, there is a drastic increase in the critical elongation rate $\dot{\varepsilon}^*$ as seen in Figure 1. This behavior is likewise seen in the case of shear flow, and is

due to the effect of hydrodynamic screening. Figure 4 provides the average flow profile surrounding a globule, and the accompanying graphs demonstrate the critical feature. Because of the interactions between the polymer and the surrounding fluid, the velocity of the fluid essentially drops to zero at the surface of an effective sphere surrounding the globule. This results in a globule that effectively becomes isolated from the surrounding flow field. The globule−stretch transition now relies on the ability of a thermal protrusion to exceed this low-flow regime and to be pulled with the external field with sufficient force to overcome the cohesive force. An example of this behavior can be seen in Movie S4 (Supporting Information). The geometry of this case is represented schematically in Figure 2c. To derive this relationship, we start with this cohesive force for a single monomer:

$$F_{coh} \sim kT\frac{\Delta\tilde{u}}{a}\left(\frac{l}{a}\right)^{\alpha-1} \tag{13}$$

where α introduces the dependence of the cohesive force on the length of the protrusion with respect to the interfacial width, with $\alpha = 1$ representing a protrusion much longer than the interfacial width, and $\alpha = 2$ representing a protrusion that is shorter than the interfacial width (the harmonic approximation). This is balanced against the hydrodynamic force on a protrusion of length l:

$$F_{prot} = {\mu_0}^{-1}\int_0^l \vec{v}(\vec{\mathrm{d}}\, l/a) \tag{14}$$

This equation requires the knowledge of the velocity profile $\vec{v}$, which we model as a hard sphere in an elongational flow profile. This can be derived using the method of Hasimoto to be:[37]

$$\vec{v} = \dot{\varepsilon}(3\delta_{\alpha z}-1)\left[r_\alpha\left(\frac{1}{2}-\frac{5R^3}{4r^3}+\frac{3R^5}{4r^5}\right) + r_z(r_z r_\alpha + ({r_x}^2+{r_y}^2-r_\alpha r_z)\delta_{\alpha z})\left(\frac{15}{4}\left(\frac{R^3}{r^5}-\frac{R^5}{r^7}\right)\right)\right] \tag{15}$$

where the constant R is the radius of the sphere. This flow profile agrees with the data obtained by the simulation, as shown in Figure 4. We will assume that the length of the protrusion l is very small compared to the overall sphere radius R, and we can thus use an expansion of this profile along the z (extensional) axis. This results in a scaling of the form:

$$F_{prot} \sim \frac{\dot{\varepsilon} l^3}{\mu_0 a R} \sim \eta\dot{\varepsilon} l^3/R \tag{16}$$

Setting this force equivalent to the cohesive force at a critical elongation rate $\dot{\varepsilon}^*$, and introducing the relationship $l \sim kT/F_{coh}$

$$\dot{\varepsilon}^*\tau \sim \frac{R\Delta\tilde{u}^{4/\alpha}}{a} \sim N^{1/3}\Delta\tilde{u}^{4/\alpha} \tag{17}$$

where we have made the replacement $R \sim N^{1/3}a$. We note that this scaling law is identical to the one given for shear flow unfolding with HI,[11,13] a result that demonstrates the similarities of both flows around the sphere.

The simulation data shown in Figure 5 presents a slightly different scaling (we will assume that in the above scaling law the interface is diffuse so we use the harmonic approximation and set $\alpha = 2$), with the log−log plot of $\dot{\varepsilon}^*\tau$ versus u demonstrating scaling relationships of $\dot{\varepsilon}^* \sim \Delta u^\beta$ and $\dot{\varepsilon}^* \sim N^0$, where β transitions from 1 to 2 depending on the interaction energy $\Delta\tilde{u}$. In analogue to the shear case, we explain this difference in the context of a partially penetrable globule. This approach is similar to the "f-shell blob" model by Rzehak et al. which demonstrated that the behavior of tethered polymers in flows could be described by blobs modeled as impenetrable beads surrounded by freely draining shells.[41] In this case, we obtain the expression for a partially penetrable sphere that provides an intermediate case between a completely shielded globule and the FD case considered above. In order to determine this, the velocity profile equation as it is used in the protrusion drag situation given above is adjusted to account for a hydrodynamic radius that is smaller than the actual polymer radius:

$$F_{prot} \sim \frac{1}{a\mu_0}\int_R^{R+l} v_z\,\mathrm{d}z \sim \frac{\dot{\varepsilon}}{2a\mu_0}\left(r^2+5\frac{{R_{HI}}^3}{r}-\frac{{R_{HI}}^5}{r^3}\right)_R^{R+l} \tag{18}$$

where R is the radius at the base of the protrusion (the globule radius), $R_{HI} = R - \lambda$ is the radius of the equivalent hydrodynamic sphere, and l is the protrusion length. In this case, if we assume that both λ and l are small, we can expand the result of this equation to obtain the scaling relationship:

$$F_{prot} \sim \frac{\dot{\varepsilon} l(\lambda^2+\lambda l+l^2/3)}{\mu_0 a R} \tag{19}$$

Notice that as we approach the condition of $\lambda \sim 0$, the we obtain eq 16. At the opposite limit of $\lambda > l$, a different scaling dominates. Reconsidering this equation in relation to the theory developed above, we obtain:

$$\dot{\varepsilon}^*\tau \sim \frac{N^{1/3}a^2\Delta\tilde{u}^{2/\alpha}}{\lambda^2} \tag{20}$$

We can again consider a broad interface that conforms to the $\alpha = 2$ harmonic approximation. By considering penetration, we see that it is expected that the scaling of $\Delta\tilde{u}$ with $\dot{\varepsilon}^*\tau$ will vary smoothly from 1 to 2 depending on the relative size of the critical protrusion length and the depth of flow penetration. This relationship is evident in our simulation results , which demonstrate a gradual shift from limiting slopes of 1 for low values of $\Delta\tilde{u}$ and 2 for high values of $\Delta\tilde{u}$. We consider that the globule at low interaction strengths is very diffuse and demonstrates the expected scaling for the $\dot{\varepsilon}^*\tau \sim \Delta\tilde{u}$ case, since there is a lot of room for solvent to penetrate the globule. Only at very high interaction energies does the globule retain a sharper interface, and the scaling starts to change toward the $\dot{\varepsilon}^*\tau \sim \Delta\tilde{u}^2$ case predicted for the non-penetrating case. Interestingly, this particular scaling argument depends very weakly on the size of the globule, and this relationship predicts that larger globules are more resilient to larger flow rates. This differs drastically from the FD case, where larger globules require less flow rate to excite a globule−stretch transition. In the transition from the HI to the FD case, however, we note that the previously derived

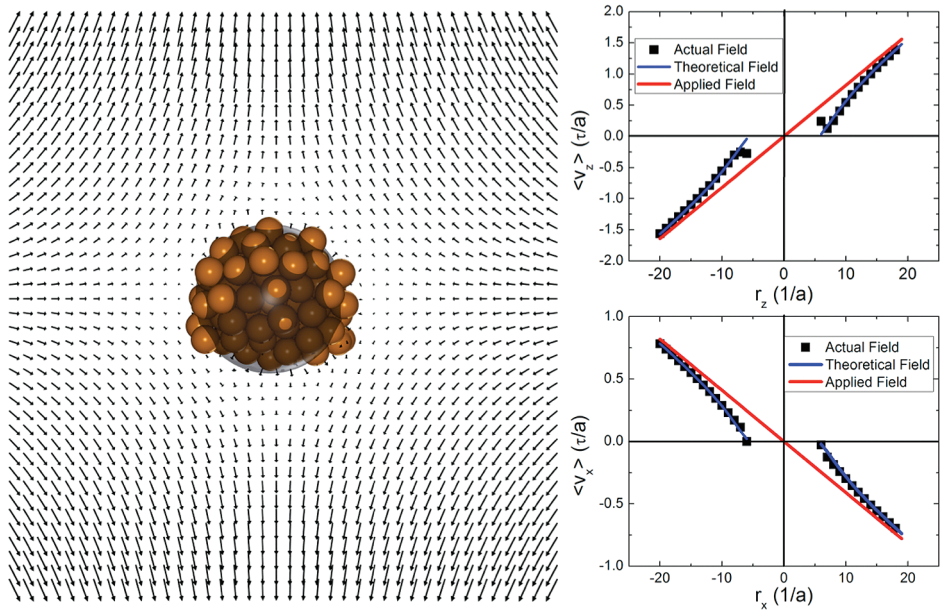

Figure 4. Average flow profile surrounding a collapsed polymer globule ($\Delta\tilde{u} = 3.0$) in a sub-$\dot{\varepsilon}^*$ elongation rate of $0.082(1/\tau)$. The graphs on the right quantitatively compare the actual flow profile obtained from the simulations and the theoretical flow profile from eq 15 to the applied elongational flow profile. The fit of the theoretical flow profile to the simulation data yields the effective hydrodynamic radius of the globule, which is indicated in the figure on the left as a translucent blue sphere. Note that the radius of the effect of hydrodynamic stagnation represented by this sphere is smaller than the radius of the actual globule, which supports our assumption of a region of flow penetration into the globule.

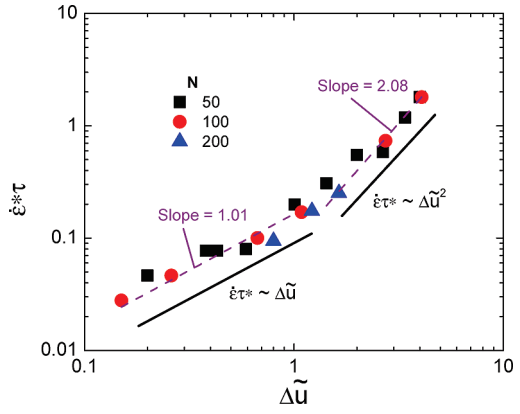

Figure 5. Scaling behavior of the critical elongation rate $\dot{\varepsilon}^*\tau$ versus the interaction energy $\Delta\tilde{u}$ taken from Brownian dynamics simulations for chains of varying length considering HI. A gradual transition between twoscaling regimes is seen, with $\dot{\varepsilon}^* \sim \Delta\tilde{u}^1$ at low interaction energies and $\dot{\varepsilon}^* \sim \Delta\tilde{u}^2$ at high interaction energies. Results are shown for $N = 50$ (black squares), $N = 100$ (red circles), and $N = 200$ (blue triangles). The dashed purple lines represent the best fit lines through the data, while the solid black lines demonstrate the slope predicted by the scaling argument. The slopes for the best fit lines are in excellent agreement with the theoretical prediction.

equations were only valid for the condition $\lambda,l \ll R$. As λ approaches R, λ becomes a function of N and the above analysis no longer holds. Upon the condition that $\lambda \sim R$, we expect the FD scaling to be obtained. One result of this transition from HI to FD, which is described for the shear case as well,[11,13] is an implicit change in the scaling of $\dot{\varepsilon}^*\tau$ with N. This explains the apparent scaling exponent of 0 seen in our simulations, as this value lies between the predicted exponent of $^1/_3$ for the HI case and -1 for the FD case.

It is instructive to compare this particular flow profile versus the behavior in shear flow as described previously by Alexander-Katz and Netz.[11,13] It is commonly understood that globules or drops in shear flows can dissipate energy by rotational motion,[13] rendering drops above a certain viscosity relative to the medium to be stable even at high shear rates. Elongational deformation has no associated vorticity, so the mechanism for energy dissipation is instead shape deformation (which effectively increases the interfacial surface area) which is a main motif of our proposed mechanism for the FD case. Also, the dynamics of a collapsed polymer in shear flow involves the presence of a tumbling movement that prevents the permanent elongation of the polymer and results in the persistent alternation between collapsed and stretched states.[5,35] In elongational flow, there is no dynamical pathway for a polymer that is stretched in a given flow rate to return to a collapsed state. This results in a permanent elongation that only explores the dynamics between the two states once for a given $\dot{\varepsilon}^*$.

Dynamics of Unfolding Collapsed Polymers. A significant amount of energy has recently been placed into the study of the unfolding dynamics of coiled polymer chains. Recent work in this field has studied this effect to provide insight into hydrodynamic effects on polymer dynamics,[38] the effect of topography on dynamics,[2,18,39,40] and other questions of fundamental significance.[3,9,10] Experimentally, this is usually done at a stagnation point in a cross-channel microfluidic setup and imaged with fluorescently labeled DNA molecules.[2,9] It has been shown that these results are very faithfully reproduced using Brownian dynamics simulations like the type we are considering.[10,33]

We simulated a series of polymers such that they undergo a step increase in the elongational flow rate $\dot{\varepsilon}$ from below to above $\dot{\varepsilon}^*$ and concurrently extend from a collapsed globule to a fully extended chain. Using this data, we can explore the correlation between the geometries of the extending chains with the dynamics to support the mechanisms proposed in the previous section. The end-to-end distance can be plotted as a function of time during this transition, which is shown for a FD system in Figure 6 for $N = 100$ at low interaction energies $\Delta\tilde{u} = 0.26$. Each curve represents a different trial at this condition. These dynamics correspond very closely to

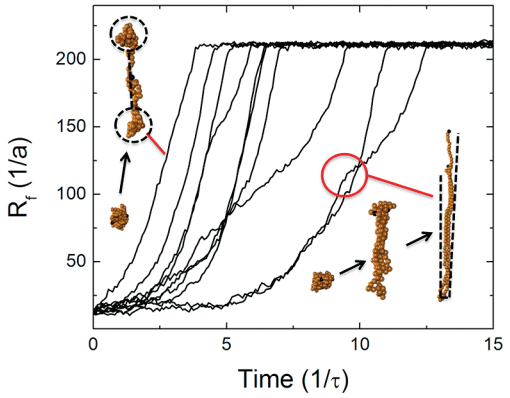

Figure 6. End-to-end distance R_F of a polymer measured as a function of time for a 100 bead chain in FD conditions (at low interaction energies, $\Delta\tilde{u} = 0.26$). They are raised from below $\dot{\varepsilon}^*$ to just above $\dot{\varepsilon}^*$ ($\dot{\varepsilon}\tau = 0.02$) at time $t = 0$. We note the presence of two distinct conformation types, and include snapshots of each from simulation data: the left shows the dumbell configuration, and the right shows the kinked conformation. The latter demonstrates a "hesitation" in the unfolding dynamics, which is indicated in the red circle. The dumbell case does not demonstrate this feature. Black dotted lines outline the basic geometries present in the simulation figures.

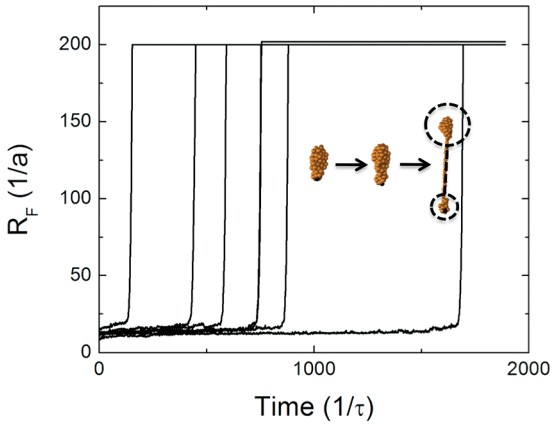

Figure 7. End-to-end distance R_F of a polymer measured as a function of time for 100 bead chains considering FD at high interaction strengths $\Delta\tilde{u} = 3.0$. They are raised from below $\dot{\varepsilon}^*$ to just above $\dot{\varepsilon}^*$ ($\dot{\varepsilon}\tau = 0.158$) at time $t = 0$. Snapshots from simulations are shown to demonstrate the typical conformations seen during unfolding. A capillary instability forms close enough to the center of the globule that the smaller lobe is able to be pulled apart from the larger one, resulting in the dumbell geometry outlined by the black dotted lines.

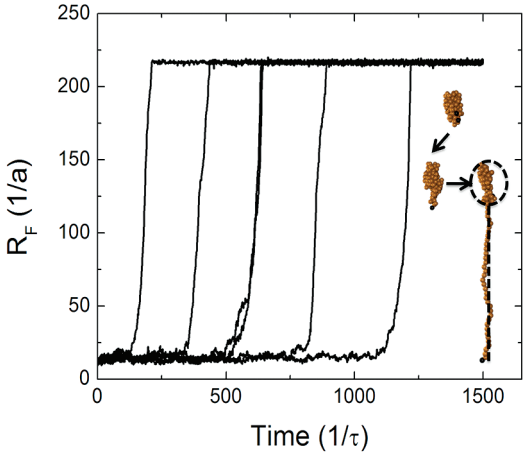

Figure 8. End-to-end distance R_F of a polymer measured as a function of time for 100 bead chains considering HI. The flow rate $\dot{\varepsilon}$ is raised from below $\dot{\varepsilon}^*$ to just above $\dot{\varepsilon}^*$ ($\dot{\varepsilon}\tau = 0.11$, $\Delta\tilde{u} = 0.67$) at time $t = 0$. Snapshots from simulations are shown to demonstrate the typical conformations seen during unfolding. A thermal protrusion extends far enough away from the globule to be pulled by the surrounding flow field, resulting in a half-dumbell geometry outlined by the black dotted lines.

the dynamics for the extension of a coiled polymer, which is presented both experimentally and computationally by Perkins et al. and Agarwal.[2,38,39] Most notably, there is an immediate response of the chain length to the step-increase in $\dot{\varepsilon}\tau$ that results in unfolding times on the order of 10τ. Because of the rapid stretching dynamics, a variety of geometries can be described that correlate to the variety in initial chain topologies. This effect has been explored in great detail by Perkins et al. and Agarwal.[2,38,39] We observe two general behaviors that are also seen in coiled polymers: folded and "dumbell" shaped geometries. An example of the folded geometry is shown in Movie S1 (Supporting Information), the dumbell geometry in Movie S2 (Supporting Information), and snapshots representing these behaviors are shown in Figure 6. Black dotted lines are used in Figure 6 as a schematic to represent the dumbell and folded geometries. We notice similar trends in the observations of Agarwal that the appearance of folds causes a "hesistation" in the stretching dynamics that represents the relative stability of such a fold to this particular flow field that occurs when both ends of the polymer are on the same side of the chain's center of mass.[38,39] An example of this behavior is demonstrated in Figure 6, and is indicated by the red circle.

The dynamics become drastically different at other conditions-the high-$\Delta\tilde{u}$ FD case and the HI case have topological constraints that promote certain unfolding geometries. These constraints are governed by the unfolding mechanisms, which also control the dynamics of unfolding. We first consider the high-$\Delta\tilde{u}$ FD case, which we have proposed an intrusion-based mechanism for. This mechanism relies on the formation of two "lobes" of unequal size through thermal fluctuations. The smaller lobe must be large enough for its drag force to overcome the surface tension holding the globule together. The balance of forces results in a nucleation−growth-type mechanism, which suggests a distribution of times at which the transition is initiated. Indeed, the stretching transition dynamics are plotted in Figure 7, and it is clear that the globule is metastable to the stretch transition on time scales much longer than the transition itself. The globule can remain collapsed to $>1000\tau$ even above $\dot{\varepsilon}^*\tau$. Snapshots from the simulation are also shown in Figure 7, demonstrating the geometries typically seen in this transition, and Movie S3 in the Supporting Information also demonstrates this feature. As predicted, two asymmetric lobes are formed and pulled apart in a dumbell geometry. The black dotted lines again form a schematic to describe this geometry.

Like the high-$\Delta\tilde{u}$ FD case, the mechanism of the HI globule−stretch transition governs the geometry and dynamics of the unfolding polymer. In the HI case, the proposed mechanism is the presence of a protrusion that is long enough to feel thedrag force necessary to overcome the globule's cohesive force. This mechanism, much like the previous case, has nucleation−growth-type dynamics. Thus, the characteristic metastability is also seen (in Figure 8), with the transition occurring as long as1000τ beyond the application of the flow above $\dot{\varepsilon}\tau$. The protrusion mechanism constrains the unfolding geometry to be a half-dumbell, as is demonstrated by the simulation snapshots shown in Figure 8 and Movie S4 (Supporting Information). This arises from

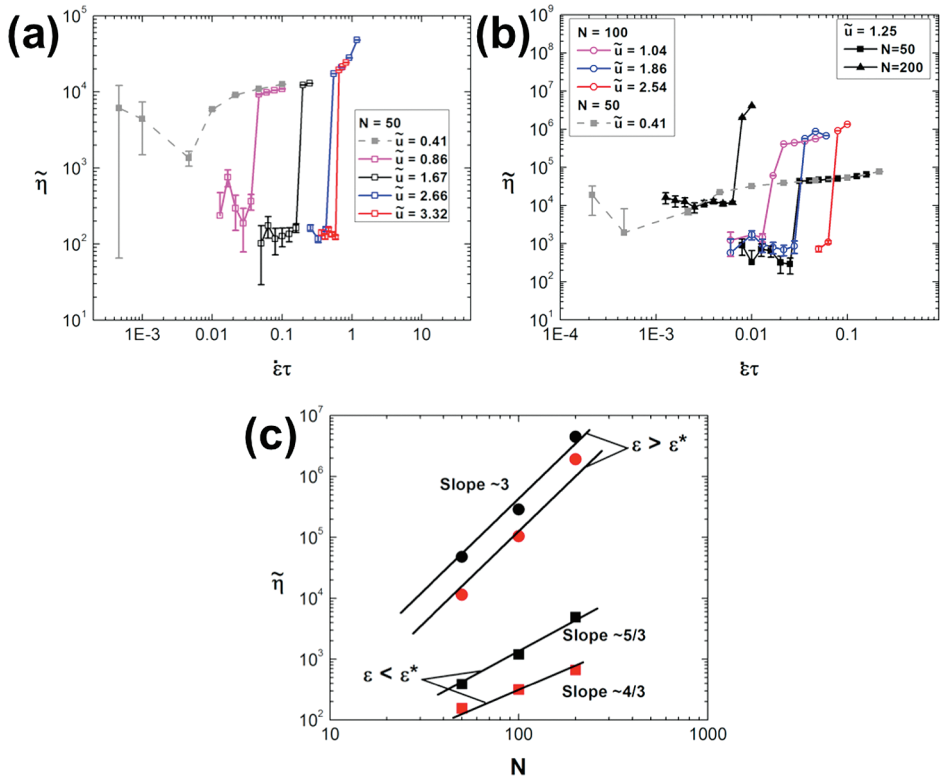

Figure 9. (a) $\dot{\eta}$ in the FD case as a function of $\dot{\varepsilon}\tau$. (b) $\dot{\eta}$ in the HI case as a function of $\dot{\varepsilon}\tau$. For both parts a and b, different colors represent different interaction energies $\tilde{u}$ while different symbols represent different chain lengths. Both parts a and b also plot both FD and HI cases respectively for the theta condition ($\tilde{u} = 0.41$) to contrast the discrete viscosity jump of the globule−stretch transition to the continuous coil−stretch transition (gray dotted lines). (c) Plot of $\dot{\eta}$ as a function of N for both FD (black symbols) and HI (red symbols) cases. Square symbols represent the average (overall simulations) value of $\dot{\eta}$ below $\dot{\varepsilon}^*$, and the circle symbols represent the average (over all simulations) value of $\dot{\eta}$ above $\dot{\varepsilon}^*$.

the typical case of the protrusion being a single chain end, as a protrusion consisting of a nonchain-end segment of the same length feels a cohesive force approximately twice as large.

Elongational Viscosity. We can analyze the elongational viscosity of globular polymers in flow. If a dilute solution (and therefore negligible globule−globule interaction) is assumed, it is sufficient to extract the viscosity from single-polymer simulations. In practice, such conditions are difficult to achieve in synthetic systems without inducing large-scale phase separation, however we expect that sufficient stabilization using (for example) electrostatics could facilitate the experimental realization of such a system. These results may have more profound implications outside the realm of synthetic polymers, however. In this article we are motivated by more complex macromolecules, like vWF which is an extremely large, soluble, yet compact (or collapsed) (bio)macromolecule. The inherent amphiphilicity of its monomers confer to it this property, which is generally true for many proteins. Ultimately, this type of system could yield insight into the mechanisms of turbulence drag reduction, in which polymers in dilute solutions are able to significantly increase the viscosity of the overall solution upon the application of high flow rates.[7,23−25] This prevents the formation of turbulence by locally decreasing the Reynold's number of the flow in highly elongating regimes.[7]

To calculate the viscosity we directly evaluate the contribution per polymer to the stress tensor π as:

$$\pi = -\frac{c}{N}\sum_{i=1}^{N}\langle \mathbf{r}_i\mathbf{F}_i\rangle \tag{21}$$

where c is the monomer density and $\mathbf{F}_i = -\nabla_{\mathbf{r}_i}U$ is the force acting on the ith bead.[42] The average is done over the time trajectory of the simulation. The contribution of the polymer to the elongational viscosity is then simply evaluated via:[17]

$$\eta_P(\dot{\varepsilon}) = \frac{\pi_{zz} - (\pi_{xx} + \pi_{yy})/2}{\dot{\varepsilon}} \tag{22}$$

Here we use an equivalent dimensionless quantity $\dot{\eta}$ that we define as:

$$\tilde{\eta} = \frac{N\eta_P}{6\pi\psi\eta_S} \tag{23}$$

where η_S and $\psi = ca^3$ correspond to the viscosity of the pure solvent and the volume fraction of polymer, respectively. From the definition of the intrinsic viscosity $[\eta]$, one sees that $\dot{\eta} \sim N[\eta]$. To study both the FD and HI cases, we have plotted value $\dot{\eta}$ versus the dimensionless elongation rate $\dot{\varepsilon}\tau$ for a variety of interaction strengths $\tilde{u}$ and chain lengths N (see Figure 9, parts a and b). Both the FD and HI cases display similar characteristics, with $\dot{\eta}$ staying roughly constant with increasing $\dot{\varepsilon}\tau$ until the critical elongation rate $\dot{\varepsilon}^*$. This provides the simple result that the stress contribution per polymer is constant with elongation rate, so long as the molecules remain in a collapsed state. This result is intuitive given the roughly constant shape of the globule. This constant value for $\dot{\eta}$ does not change significantly with $\tilde{u}$, and is averaged over all simulations for a given chain size N. This is plotted in Figure 9 (c) for both HI and FD cases. Both give slightly different scalings-the FD case has a scaling of $\dot{\eta} \sim N^{5/3}$, which can be explained by the geometric consideration

of the drag force upon the beads integrated over the volume of a sphere as a way of approximating the discrete Kirkwood−Riseman equation:

$$\eta \sim N\eta_P \sim \frac{\sum_{i=1}^{N} \langle r_z F_z - (r_x F_x + r_y F_y)/2\rangle}{\dot{\varepsilon} a^3} \sim \frac{\int_V r\eta_S a\dot{\varepsilon} r \, \mathrm{d}V}{\dot{\varepsilon} a^3} \sim \eta_S a^{-5} r^5 \sim \eta_S N^{5/3} \quad (24)$$

which is the scaling obtained in the simulations. The HI case has a scaling of $\dot{\eta} \sim N^{4/3}$, which can be explained by considering a similar integration as above, only over the surface of the sphere to discount the hydrodynamically shieldedbeads in the center of the sphere:

$$\eta \sim N\eta_P \sim \frac{\sum \langle r_z F_z - (r_x F_x + r_y F_y)/2\rangle}{\dot{\varepsilon} a^3} \sim \frac{\int_S r\eta_S a\dot{\varepsilon} r \, \mathrm{d}S}{\dot{\varepsilon} a^3} \sim \eta_S a^{-4} r^4 \sim \eta_S N^{4/3} \quad (25)$$

which is the scaling obtained in the simulations (see Figure 9c). Upon reaching the globule−stretch transition (see Figure 9), there is a discrete jump to what is roughly a constant value of $\dot{\eta}$ (the concurrent upswing is an artifact of our model, which uses simple springs to connect beads, rather than a more accurate FENE potential). Besides the artifacts introduced by our model, the value of $\dot{\eta}$ is roughly constant upon elongation, again a function of the constant shape of the globule. At lower elongation rates (though still above $\dot{\varepsilon}^*\tau$), the asymptotic value is plotted in Figure 9c for both HI and FD, and follows the scaling law $\dot{\eta} \sim N^3$. This follows from purely geometric considerations:

$$\eta \sim N\eta_P \sim \sum_N \frac{\langle r_z F_z\rangle}{\dot{\varepsilon} a^3} \sim \frac{\int_0^N z(\dot{\varepsilon}\eta_S a z) \, \mathrm{d}z}{\dot{\varepsilon} a^3} \sim \eta_S N^3 \quad (26)$$

where the discrete Kirkwood equation was approximated as an integral over the length of the chain and the velocity profile (proportional to the force) along the chain. These simulation results are nearly identical to those for fully extended chains in similar studies of coiled polymers, a result that is expected due to the equivalent geometry of both situations.[17] The only apparent difference between the FD and HI case is in the magnitude of the dimensionless viscosity, which is less in the HI case due to the hydrodynamic screening.

The interesting result for the viscosity of dilute collapsed polymers is the large discrete jump upon exceeding the critical elongation rate, which quickly becomes quite potent upon introduction of polymers of increasing length. This describes the potential for using collapsed polymers in the case of turbulence drag reduction, or other cases where discrete (and highly tunable) jumps in solution velocity are desired. This is further aided by the lack of dependence of the discrete globule−stretch transition(assuming the HI case) on the chain size. Thus, very controllable systems can potentially be created out of polydisperse polymers. The controllable parameter for these systems would be the strength of self-interaction of the polymer. It is conceivable that, using this method, solutions with a distribution of polymer self-interaction strengths could be provided with highly tunable elongational viscosities.

Conclusions

We have demonstrated using Brownian dynamics simulations the presence, nature, and dynamics of the globule to stretch transition of a collapsed polymer in the presence of an extensional flow field. This provides, coupled with previous research considering shear flow, compelling insight into the behavior of collapsed polymers in flowing dilute solutions. We have identified, and supported with a simple scaling theory, a likely mechanism for the globule−stretch transition which is based on the typical lengthof protrusions due to thermal fluctuations. Particularly important for this effect is the shielding due to hydrodynamic interactions, which results in the collapsed globule behaving as an effective hard-sphere. Only by allowing protrusions to extend beyond the shielded area does the fluid exert enough stress to stretch the molecule to its full contour length.

Furthermore, the dynamics of this stretching transition are well characterized and follow kinetics similar to the analogous process for a coiled polymer. Topology plays a key role, with the appearance of folds hindering the stretching process. This also yields insight into the mechanistic nature of the stretch transition, with a distinct lack of folds and a presence of a long-time scale metastability as soon as hydrodynamic interactions were included due to the topographically limiting unfolding process as a result of the protrusion-nucleation.

This fundamental research provides insight into the unfolding nature of certain proteins in biology. In particular, proteins such as von Willebrand Factor that are critical in the blood clotting process are known to be strongly dependent on flow conditions. We hypothesize that this mechanism is a key factor in such biological processes, and an understanding of this process could provide guidance in the further manipulation of these systems for medical purposes. One particularly interesting insight arises from the consideration of actual values based on the structure of vWF. In our previous work with shear flows,[13] there is an order-of-magnitude analysis that places the shear transition of a polymer with $a = 100$ nm at a value of $\dot{\gamma} \sim 1000\ \mathrm{s}^{-1}$. Using a similar order-of-magnitude analysis (for $\Delta\tilde{u} \sim 2$ and $\dot{\varepsilon}\tau \sim 1$), we can use the typical monomer size of vWF $a = 100$ nm to obtain the value of $\dot{\varepsilon} \sim 20\ \mathrm{s}^{-1}$. Thus, there is approximately 1 or 2 orders of magnitude difference between the flow rates necessary to extend a globule via shear versus via elongation. This suggests an explanation for the behavior seen in recent investigations that reveal that gradient shearflows enhance blood clotting behavior,[27] as gradient shear flows have a significant elongational component.

Practical applications in fluid control are also apparent, with a highly useful discretized viscosity response seen in the extrapolation of single-molecule simulations to dilute solution properties. This may allow for the creation of highly tunable fluidsthat display unique and otherwise unattainable viscosity responses to elongational flow fields.

Acknowledgment. The authors acknowledge funding provided by the Dupont−MIT Alliance.

Supporting Information Available: Movies of folded versus dumbell topologies in unfolding polymers (100 beads, $\dot{\varepsilon} = 0.02$, $\tilde{u} = 0.84$ and 3.00, freely draining) as well as movies of half-dumbell topologies in unfolding polymer including hydrodynamic interactions (100 beads, $\dot{\varepsilon} = 0.11$, $\tilde{u} = 1.25$). This material is available free of charge via the Internet at http://pubs.acs.org.

References and Notes

(1) Schroeder, C. M.; Shaqfeh, E. S. G.; Chu, S. *Macromolecules* **2004**, *37*, 9242.
(2) Perkins, T. T.; Smith, D. E.; Chu, S. *Science* **1997**, *276*, 2016.
(3) Doyle, P. S.; Shaqfeh, E. S. G. *J. Non-Newton. Fluid* **1998**, *76*, 43.
(4) Shaqfeh, E. S. G. *J. Non-Newton. Fluid* **2005**, *130*, 1.
(5) de Gennes, P. G. *J. Chem. Phys.* **1974**, *60*, 5030.
(6) Gupta, R. K.; Nguyen, D. A.; Sridhar, T. *Phys. Fluids* **2000**, *12*, 1296.

(7) Larson, R. G. *J. Non-Newton. Fluid Mech.* **2003**, *111*, 229.
(8) Kim, J. M.; Doyle, P. S. *Lab Chip* **2007**, *7*, 213.
(9) Balducci, A. G.; Tang, J.; Doyle, P. S. *Macromolecules* **2008**, *41*, 9914.
(10) Larson, R. G.; Hu, H.; Smith, D. E.; Chu, S. *J. Rheol.* **1999**, *43*, 267.
(11) Alexander-Katz, A.; Schneider, M. F.; Schneider, S. W.; Wixforth, A.; Netz, R. R. *Phys. Rev. Lett.* **2006**, *97*, 138101.
(12) Alexander-Katz, A.; Netz, R. R. *Europhys. Lett.* **2007**, *80*, 18001.
(13) Alexander-Katz, A.; Netz, R. R. *Macromolecules* **2008**, *41*, 3363.
(14) Schneider, S. W.; Nuschele, S.; Wixworth, A.; Gorzelanny, C.; Alexander-Katz, A.; Netz, R. R.; Schneider, M. F. *Proc. Natl. Acad. Sci. U.S.A.* **2007**, *104*, 7899.
(15) Goto, S.; Salomon, D. R.; Ikeda, Y.; Ruggeri, Z. M. *J. Biol. Chem.* **1995**, *270*, 23352.
(16) Hur, J. S.; Shaqfeh, E. S. G.; Larson, R. G. *J. Rheol.* **2000**, *44*, 713.
(17) Neelov, I. M.; Adolf, D. B.; Lyulin, A. V.; Davies, G. R. *J. Chem. Phys.* **2002**, *117*, 4030.
(18) Venkataramani, V.; Sureshkumar, R.; Khomami, B. *J. Rheol.* **2008**, *52*, 1143.
(19) Liu, S.; Ashok, B.; Muthukumar, M. *Polymer* **2004**, *45*, 1383.
(20) Hernandez Cifre, J. G.; Garcia de la Torre, J. *J. Rheol.* **1999**, *43*, 339.
(21) Harrison, G. M.; Remmelgas, J.; Leal, L. G. *J. Rheol.* **1998**, *42*, 1039.
(22) Jendrejack, R. M.; de Pablo, J. J.; Graham, M. D. *J. Chem. Phys.* **2002**, *116*, 7752.
(23) Warholic, M. D.; Massah, H.; Hanratty, T. J. *Exp. Fluids* **1999**, *27*, 461.
(24) Orlandi, P. *J. Non-Newton. Fluid* **1995**, *60*, 277.
(25) Den Toonder, J. M. J.; Hulsen, M. A.; Kuiken, G. D. C.; Nieuwstadt, F. T. M. *J. Fluid Mech.* **1997**, *337*, 193.
(26) Stone, H. A. *Annu. Rev. Fluid Mech.* **1994**, *26*, 65.
(27) Nesbitt, W. S.; Westein, E.; Tovar-Lopez, F. J.; Tolouei, E.; Mitchell, A.; Fu, J.; Carberry, J.; Fouras, A.; Jackson, S. P. *Nat. Med.* **2009**, *15*, 665.
(28) Stone, H. A.; Bentley, B. J.; Leal, L. G. *J. Fluid Mech.* **1986**, *173*, 131.
(29) Stone, H. A.; Leal, L. G. *J. Colloid Interface Sci.* **1989**, *133*, 340.
(30) Stone, H. A.; Leal, L. G. *J. Fluid Mech.* **1989**, *198*, 399.
(31) Rotne, J.; Prager, S. *J. Chem. Phys.* **1969**, *50*, 4831.
(32) Yamakawa, H. *J. Chem. Phys.* **2003**, *53*, 436.
(33) Larson, R. G. *J. Rheol.* **2005**, *49*, 1.
(34) Alexander-Katz, A.; Wada, H.; Netz, R. R. *Phys. Rev. Lett.* **2009**, *103*, 028102.
(35) Smith, D. E.; Babcock, H. P.; Chu, S. *Science* **1999**, *283*, 1724.
(36) Buguin, A.; Brochard-Wart, F. *Macromolecules* **1996**, *29*, 4937.
(37) Hasimoto, H. *J. Phys. Soc. Jpn.* **1992**, *61*, 3027.
(38) Agarwal, U. S. *J. Chem. Phys.* **1998**, *108*, 1610.
(39) Agarwal, U. S. *J. Chem. Phys.* **2000**, *113*, 3397.
(40) Larson, R. G. *Rheol. Acta* **1990**, *29*, 371.
(41) Rzehak, R.; Kienle, D.; Kawakatsu, T.; Zimmermann, W. *Europhys. Lett.* **1999**, *46*, 821.
(42) Doi, M.; Edwards, S. F. *The Theory of Polymer Dynamics*; Oxford University Press: New York, 1986.